Journal of Thermal Analysis and Calorimetry, Vol. 72 (2003) 299–310

TEXTURE OF ZIRCONIA OBTAINED BY FORCED HYDROLYSIS OF $ZrOCl_2$ SOLUTIONS
Influence of aging on thermal behavior

P. Jakubus[1*], *A. Adamski*[2], *M. Kurzawa*[1] *and Z. Sojka*[2]

[1]Szczecin Technical University, Institute of Chemistry and Environment Protection, al. Piastów 42, 71-065 Szczecin, Poland
[2]Jagiellonian University, Faculty of Chemistry, Ingardena 3, 30-060 Cracow, Poland

Abstract

The structure and surface properties of ZrO_2 strongly depend on its preparation. In the present work the impact of prolonged aging at basic conditions (pH = 9, T = 100°C, t = 48 h), on the phase composition and textural properties, obtained by calcination of the precipitate, was investigated using several techniques conjointly (DTA/TG, DSC, XRD, porosimetry). The thermal effects accompanying the $ZrO_2 \cdot xH_2O$ gel formation, the coalescence of the particles and crystallization were evaluated and discussed in terms of the structural differences between the aged and non-aged samples.

Keywords: aging, coalescence, crystallization, DSC, DTA/TG, hydrous zirconia, nucleation, phase transitions, porosimetry, tetragonal zirconia stabilization, XRD,

Introduction

Growing interest in zirconia, evolving in the last decade, is undoubtedly related to the increasing number of its actual and potential technological applications. Zirconium oxide can be used as catalyst and catalyst support [1–3] , high-performance material for production of refractories, fuel cells, oxygen sensors and neo-ceramic tools [4–6]. All these applications are possible owing to the very particular chemical, thermal and mechanical properties of zirconia. Recently, the preparation of thermally-stable mesoporous zirconia possessing high surface area (> 350 m^2g^{-1}) and well ordered pore structure of relatively narrow pore size distribution has became possible due to substantial progress in the development of the preparation techniques [7, 8]. Such materials are extremely attractive for heterogeneous catalysis.

One of the characteristic features of ZrO_2 is: its existence in various polymorphic forms (monoclinic $P2_1/c$, tetragonal $P4_2/nmc$ and cubic Fm3m) of distinctly different bulk and surface properties. Although at ambient conditions for coarse grained materials the monoclinic (m-ZrO_2) form is more stable than the tetragonal (t-ZrO_2) one, in the case of fine grained samples, if the particle size r is lower than the critical value of $r_o \sim 30$ nm,

* Author for correspondence: E-mail: jakubus@ps.pl

1388–6150/2003/ $ 20.00
Akadémiai Kiadó, Budapest

t-ZrO_2 becomes thermodynamically more stable ($\Delta G(r < r_o)_{m\to t} = 4/3\pi r^3 \Delta G_{bulk} + 4\pi r^2(\gamma_t - \gamma_m) < 0$) because it exhibits considerably lower surface energy ($\gamma_t < \gamma_m$).

For catalytic applications of zirconia appropriate textural properties such as high surface area, well-developed pore structure in micro- and mesoporous regions that they are resistant to sintering are of vital importance. Surface properties and catalytic activity are also affected by the crystal form of ZrO_2, therefore the phase composition of zirconia should be controlled while engineering catalysts for the desired applications. However, during preparation of ZrO_2 by the conventional precipitation from aqueous solutions of the precursor zirconyl salt, usually a mixture of the monoclinic and tetragonal forms is produced. Therefore the use of more adequate preparation procedures leading specifically to the desired form of zirconium oxide has to be applied [9, 10].

The aim of this work is to evaluate the influence of the concentration of stock zirconyl solutions and aging of the precipitate on the crystallization of hydrous zirconia gel and the structure and textural properties of the resultant ZrO_2 obtained by subsequent calcination. The progress of the involved transformation processes was followed by differential thermal analysis, scanning calorimetry and X-ray powder diffraction techniques, corroborated by electron microscopy.

Experimental

Hydrous zirconia was obtained by precipitation from aqueous solutions of zirconyl chloride ($ZrOCl_2 \cdot 8H_2O$, Aldrich) of various concentrations (0.006, 0.02, 0.06, 0.2 and 0.6 M) with 25 % NH_3. Samples were prepared in two different ways. In the so-called acidic method, ammonia was added to the $ZrOCl_2$ aqueous solution, while in basic method this sequence was opposite. The aging of the precipitate was carried out at 100°C for 48 h in glass or Teflon beakers. In every experiment, the pH of the solutions were kept constant at ~9 during the whole treatment. The resultant zirconia gel was washed with dilute NH_4NO_3 solution until it showed negative test for Cl^- ions, filtered, then dried at 100°C for 24 h, and finally calcined in air at 600°C for 6 h.

XRD measurements were carried out by means of a Philips PW 1820 and DRON diffractometers using CoK_α radiation. For the variable-temperature experiments (VT-XRD) the samples were heated *in situ* in an Anton Parr HTK high-temperature cell. Rietveld analysis of the XRD patterns was performed with the DBWS-9411 program. Phase composition of the samples were determined from the following relationship [2]:

$$x_m = \{I_m(111) + I_m(11\bar{1})\}/\{I_m(111) + I_m(11\bar{1}) + I_t(111)\} \text{ and } x_t = 1 - x_m,$$

where I_m and I_t stand for the intensity of the corresponding monoclinic and tetragonal diffraction peaks.

Differential thermal analysis and thermogravimetry (DTA/TG) as well as differential scanning calorimetry (DSC) were carried out in aluminum pans in nitrogen or helium flow, using a SDT 2960 and a DSC 2010 (TA Instruments) apparatus, respectively. The standard heating rate was 10 K min^{-1}, while for variable-heating-rate experiments, typically rates from 2 to 25 K min^{-1} were applied.

The N_2 adsorption-desorption isotherms were measured at liquid nitrogen temperature using a Micromeritics ASAP 2010 system. Prior to the measurements, the samples were outgassed at 350°C for 10 hours. The specific surface areas were determined according to the BET method [11]. The pore volume and size distribution were calculated from adsorption isotherms based on the Barrett-Halenda-Joyner (BHJ) [12] and Horvath-Kawazoe (HK) [13] formalisms for meso- and micropores, respectively.

The SEM microstructural analysis was performed by using a JEOL JSM-1600 microscope, equipped with an ISIS 300 (Oxford) microanalyzer. Transmission electron microscopy (TEM) was carried out, using a Philips CM 20 instrument, operating at 20 kV and equipped with an EDAX system. The specimens were prepared by depositing the powder samples, dispersed in ethanol, on a holey carbon film supported on a copper grid. The size of the particles (an average diameter of the most exposed 40 – 60 particles) was assessed from the corresponding SEM/TEM micrographs.

Results and discussion

Phase composition and morphology of ZrO_2

The XRD patterns of the aged and non-aged samples, prepared from $ZrOCl_2$ solutions of the same concentration (0.6 M) in two different ways, are shown in Fig. 1. Except of the aged sample obtained by the acidic method, which was purely tetragonal (Fig. 1a) the others were mixtures of the monoclinic and tetragonal zirconia (Figs. 1b-1d), as it can be inferred from the diagnostic 2θ region between 31 and 38°. The observed lines can be attributed to the (111) reflection of the tetragonal phase (marked with *T*) and to the $(11\bar{1})$ and (111) reflections of the monoclinic phase (marked with M) [2]. The content of the tetragonal polymorph changes from 20.5 % – the non-aged ZrO_2 prepared via acidic method (Fig. 1d) – to 100 % the aged sample obtained at the constant pH = 9.3 (Fig. 1a). It is always higher for the aged samples in comparison to the raw ones. Thus the acidic

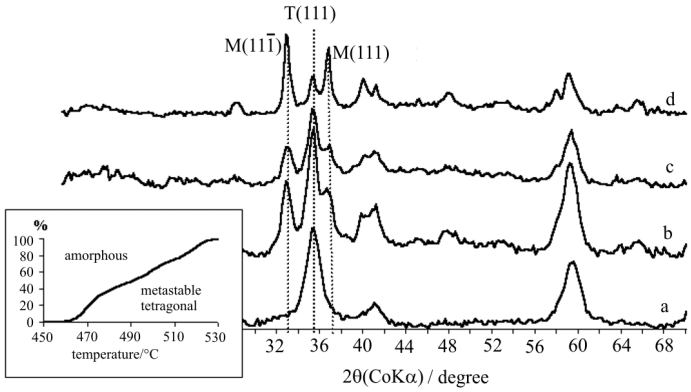

Fig. 1 Phase composition of ZrO_2 obtained by precipitation from 0.6 M solution of $ZrOCl_2$ at various preparation conditions: a – acidic method followed by ageing, b – basic method and non-aged, c – basic method and non-aged, d – acidic method and non-aged. In the insert progress of the crystallization of the sample a) is shown.

method of preparation followed by prolonged aging at 100°C is the best way to obtain pure metastable *t*-ZrO_2 upon calcination of the $ZrO_2 \cdot xH_2O$ gel at 600°C for 6 h. The crystallization progress of the zirconia gels prepared by this way was followed by the VT-XRD techniques as it is shown in the insert. The sample remains amorphous until 450°C and the crystallization into *t*-ZrO_2 is accomplished when the temperature of 530°C has been reached. This transformation is quite an involved one and entails several mutually related structural processes discussed in more detail elsewhere [14, 15].

The mechanism of the formation of hydrous zirconia and changes induced by aging can be best discussed in terms of aqueous chemistry of oxides, based on the partial charge model [16]. When $ZrOCl_2 \cdot 8H_2O$ is dissolved in water, tetramer $[Zr(OH)_2 \cdot 4H_2O]_4^{8+}$ complexes are formed as the dominant entities. Adding excess of ammonia to the $ZrOCl_2$ solution results in dramatic changes of pH, which varies from 1 up to 9.4. In such conditions the tetramers undergo hydrolysis by releasing protons from the coordinated water molecules [17].

$$[Zr(OH)_2 \cdot 4H_2O]_4^{8+} \rightarrow [Zr(OH)_{2+n} \cdot (4-n)H_2O]_4^{(8-4n)+} + 4nH^+.$$

The proton exchange between the tetramer of the mean electronegativity χ_h and the aqueous solution of pH dependent electronegativity χ_w takes place until both values become equal ($\chi_h = 2.732 - 0.035$ pH). Polymerization of the resultant species *via* olation and oxolation leads to reticulation of the tetrameric units and formation of primary particles of hydrous zirconia gel $[Zr(OH)_{8-nx}(OH)_{2x} \cdot nH_2O]$, when the critical size of nucleation is reached. The primary particles tend to coagulate forming secondary particles in order to decrease their excess energy. This process occurs either through homocoagulation between primary particles or *via* heterocoagulation between the primary particles and large aggregates [18]. However, the actual precipitate exhibited more complex structure as the secondary particles agglomerated to form larger micron-size grains (110 μm) revealed by SEM.

High basicity and elevated temperature of the solution during the aging foster partial leaching of silica from the walls of the glass beaker. The released siliceous species can be incorporated next into the precipitate network and indeed the presence of 0.02 wt.% of silicon in the samples aged at 100°C for 24 h were revealed by ICP-AES chemical analysis. This dopant, even in minute amount influences the phase composition of zirconia favoring the formation of tetragonal polymorph. This was confirmed independently in a separate model experiment, where the aging was carried out in a Teflon beaker with controlled amounts of hydrous silicon oxide (obtained by dissolving aerosil in the concentrated NH_3), added into the ageing solution intentionally [19]. It has been found that the *t*-ZrO_2 content in the sample augmented as the Si concentration was increased, and at the level of 0.02 – 0.05 wt.% of Si retained in the ZrO_2 matrix practically pure tetragonal form was obtained upon the calcination.

The BET surface areas, measured for ZrO_2 prepared in acidic way and calcined at 600°C for 6 h, are equal to $S = 23.2 \pm 0.1$ m^2g^{-1} for the non-aged sample and $S = 77.0 \pm 0.2$ m^2g^{-1} for the sample aged at 100°C for 24 h. Over three-fold increase in the specific surface area, observed in the latter case that can be explained by distinct decrease of the particle size leading to the surface area and pore structure development

(*vide infra*). The particle size established from TEM micrographs for the aged *t*-ZrO_2 was monomodal with a maximum at ca. 15 nm, while for the corresponding raw ZrO_2 it showed a broad bimodal distribution ranging from 30 to 70 nm. These results are in accordance with thermodynamic attribution of the enhanced stabilization of the *t*-ZrO_2 polymorph to the particle size effect. As it was already mentioned, an opposite decrease of the surface free energy on passing from monoclinic to tetragonal structure for crystallites with diameters smaller than the critical size of ~30 nm provides the driving force for stabilization of the latter form [20, 21]. In our case, the particles of the aged *t*-ZrO_2 were twice smaller than the reported critical size and distinctly smaller than those observed for the non-aged zirconia, consisting of a mixture of both *t*-ZrO_2 and *m*-ZrO_2 polymorphs.

In order to get insight into the texture of the samples, nitrogen sorption isotherms were measured for the non- and aged zirconia. The results revealed that both samples were porous and the corresponding isotherms are shown in the inserts of Fig. 2. In the case of the aged samples the micropores exhibited a maximum at the diameter of 0.51 nm, while the mesopores showed two maxima: a narrow one at 15 nm and a broad band ranging from 40 to 200 nm. For the non-aged samples the porosity was considerably suppressed and only regular mesopores with the diameter shifted down to 11 nm were observed. The BHJ and HK pore size distributions for micro- and mesopores are depicted in Fig. 2.

The observed adsorption isotherms are of type IV according to IUPAC classification and are characteristic of mesoporous solids [22]. From the inspection of both isotherms it can be inferred that the capillary condensation occurred with no retention of the adsorbate at low p/p_o and the hysteresis loops represented H2(E) or H1(A) [23] types for the non- and aged samples, respectively. In the latter case the closure point

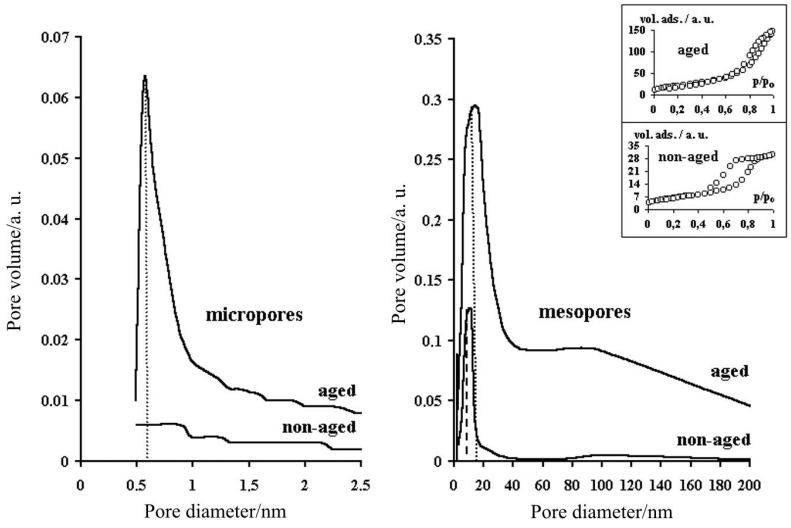

Fig. 2 Pore structure and the associated N_2-sorption isotherms for the aged and non-aged samples obtained *via* acidic method

of the loops was shifted to higher p/p_o values. The H1 hysteresis was apparently narrower than the H2 one indicating that for the aged samples the condensation took place within regular pores of cylindrical shape that are opened from both sides. In the case of the raw ZrO_2 specimens the increasing size of the loop pointed to a pronounced retention effect. Emptying the pores took place at the pressure of $p/p_o = 0.45$, *i. e*. when the meniscus became unstable, and it shifted to $p/p_o = 0.60$ for the aged ZrO_2. This indicated that the pores of the non-aged zirconia exhibited bottle shapes and they were closed, narrower and probably much more deformed [24].

Aging involved strong changes in the gel structure, enhancing the pore volume from $V_p = 0.046$ cm^{3}g^{-1} (observed for the non-aged sample) to $V_p = 0.214$ cm^{3}g^{-1}. The corresponding changes in the relative porosity of the samples, defined as $d_T V_p /(1 + d_T V_{p,})$, varied from 22 to 57% , where d_T is the theoretical density of the tetragonal ZrO_2. The enhanced porosity through increase of the surface area apparently helps in stabilization of the *t*-ZrO_2 form. The ageing also distinctly improved the sample's textural properties. As it can be inferred from the micro- and mesopores distributions, the porosity became clearly more regular and almost monomodal upon such treatment. Conceivably, when hydrous ZrO_2 gel is calcined the defective structure of the samples prepared without aging tends to collapse more readily than the more ordered and rigid lattice of the aged samples. The microporosity of the samples most likely arises from the vacancies left on removal of water during calcination of the samples, as it was earlier suggested by Sing *et al.* [25].

Thermal analysis of raw and aged zirconia gel

The DTA profiles recorded for the non-aged and aged samples precipitated from the solutions $ZrOCl_2$ of various concentrations, ranging from 0.06 to 0.6 M, are shown in Fig. 3. The averaged relative mass losses corresponding to three main transformation steps that were manifested in the curves are shown at positions indicated with the dotted vertical lines. For the non-aged samples the DTA curves were quite similar in shape, exhibiting in all cases a strong exotherm between 380 and 450°C. This peak gained in intensity and shifted toward lower temperatures with the increasing concentration of the parent zirconium solution, but was almost extinguished in the case of the aged samples. Although such strong exothermic peak in the DTA curves, sometimes termed a glow phenomenon, is often related with the crystallization of amorphous ZrO_2 [26, 27], such assignment is still debated, and alternative explanations can be found in the literature. Silva *et al*. suggested that glow effect is due to the relaxation of microstrain accumulated in large domains of zirconium hydroxyoxide [28]. Srinivasan and Davis, in turn, pointed out that crystallization and the glow phenomenon are two distinctly separate events [29]. The glow is associated with the energy release due to coalescence of the particles that is not necessarily concomitant with the proper crystallization identified with the development of a long range reticular order.

The transformation of the zirconia gel – obtained from aqueous solution by precipitation – into the corresponding oxide is a cooperative process entailing dehydration, dehydroxylation, olation/oxolation and nucleation steps followed by particle

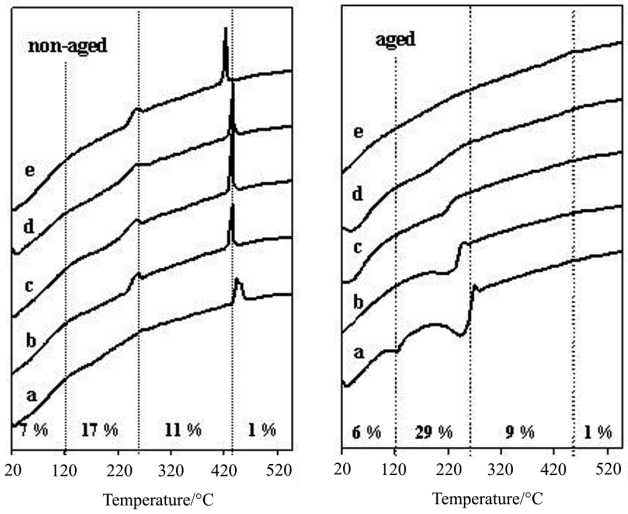

Fig. 3 DTA/TG profiles of the zirconia precipitate obtained by acidic method from $ZrOCl_2$ solutions of various concentrations: a – 0.006 M, b – 0.02 M, c – 0.06 M, d – 0.2 M, e – 0.6 M

growth. It is accomplished around 420–440°C, and above these temperatures no further significant mass decline (exceeding 1%) was observed. From the complementary XRD results (shown in the insert in Fig. 1) it is clear that the transition from amorphous to tetragonal zirconia occurred in distinctly higher temperature range 470–520°C. Therefore we think that the observed exothermic effect should rather be attributed to coalescence of the primary particles into larger ZrO_2 unites with the consequent release of surface energy. First-principle investigations showed that the surface energy of zirconium oxide is considerably anisotropic with the (111) facets being the most stable for *t*-ZrO_2 [30]. This suggests that it strongly depends on the morphology of the particles. By eroding preferentially high energy faces, prolonged aging of the precipitate led to the change of the shape of particles (revealed in TEM pictures). Because upon interfacial dissolution the (111) planes tended to be the most exposed spontaneously, the surface energy should be lowered and the associated thermal effect largely attenuated in the case of such samples, as it was observed experimentally. On the other hand, the higher was the concentration of the $ZrOCl_2$ solution the easier was the nucleation and as a result, the particle's size was smaller. The enhanced surface area is therefore most probably responsible for a weak exothermic bump observed in the case of the aged sample obtained *ex* 0.6 M solution.

Finally, basing on the results of the XRD line broadening analysis, which takes into account both the grain size and microstrain effects, we are disfavoring the attribution of the observed exothermic effect to strain relief, because in our experiment the aged samples exhibited considerably higher strain level ($\varepsilon = 0.025–0.03$) in comparison with the non-aged one ($\varepsilon = 0.015–0.02$).

The second exothermic effect, observed on DTA curves between 260 and 280°C, was less pronounced and its maximum tended to shift toward lower temperatures with the increasing concentration of the $ZrOCl_2$ solution for both samples. This exotherm was preceded by a broad endothermic peak that was best developed in the case of the aged samples obtained from the most diluted solutions. Parallel loss of the mass by 11 and 9% was observed for the raw and the aged specimens, respectively, and can be associated with elimination of water according to the equation

$$[Zr_4O_{(8-x)}(OH)_{2x}\cdot yH_2O]_n \rightarrow [Zr_4O_{(8-x)}(OH)_{2x}]_n + wH_2O$$

where x, y, n and w depend on the preparation method), followed by dehydroxylation

$$[Zr_4O_{(8-x)}(OH)_{2x}]_n \rightarrow ZrO_2 + zH_2O$$

(endothermic processes) and oxolation of hydroxyl groups

$$Zr–OH + OH–Zr \rightarrow Zr–O–Zr + H_2O$$

(exothermic process) to form embryonic oxide nuclei [9, 31]. From the corresponding mass losses – observed below 260°C – approximate formulas of the hydrous precursor ($ZrO(OH)_2\cdot 3H_2O$) and the dehydrated sample ($ZrO(OH)_2$) can be assessed.

The endothermic peak observed below 120°C (Fig. 3) was accompanied by the mass loss of 35% (aged samples) and 24% (non-aged samples) that can be associated with the elimination of molecular water physisorbed on the surface and/or occluded within the pores. From the TG data the average total mass loss of the non-aged samples was equal to 36%, while for the aged specimens it was considerably higher, reaching 45%. Upon subtracting the mass corresponding to the adsorbed water, the contents correspond to $[Zr_4O_3(OH)_{10}\cdot 10H_2O]$ and $[Zr_4O_3(OH)_{10}\cdot 17.5H_2O]$ stoichiometries of the raw and aged samples, respectively. This indicates that the latter was more hydrated, because during the aging some oxo-bridges were reverted back into hydroxyl bridges due to partial deoxolation and reolation. Such processes improve the structural order of the zirconia gel providing a molecular framework for development of the crystal structure characteristic of *t*-ZrO_2 after the calcination.

Further insight into the thermal behavior of the samples can be gained from the analysis of the DTA and DSC curves recorded as a function of the heating rate (Fig. 4). The temperatures of the principal thermal effects identified on the DTA curves remained in good agreement with those revealed by DSC and are in line with previous literature data [32, 33, 34]. Generally, the peaks due to the aged zirconia were distinctly broader than those observed for the non-aged samples. As it can be expected, with the increasing heating rate they all shifted toward higher temperatures. Slow heating (2 and 5 deg min^{-1}) allowed to determine, with better accuracy, the temperature of physisorbed water elimination, which was distinctly higher for the aged samples (~90°C) than for the non-aged ones (~50°C). Apparently water molecules nested within the hydrous zirconia framework of the aged samples are more strongly bound that those present in the fresh samples. The endothermic peak was followed by a complex thermal profile occurring between 220 and 310°C, which was actually a superposition of the endo- and exothermic events better resolved by DSC. Finally, in

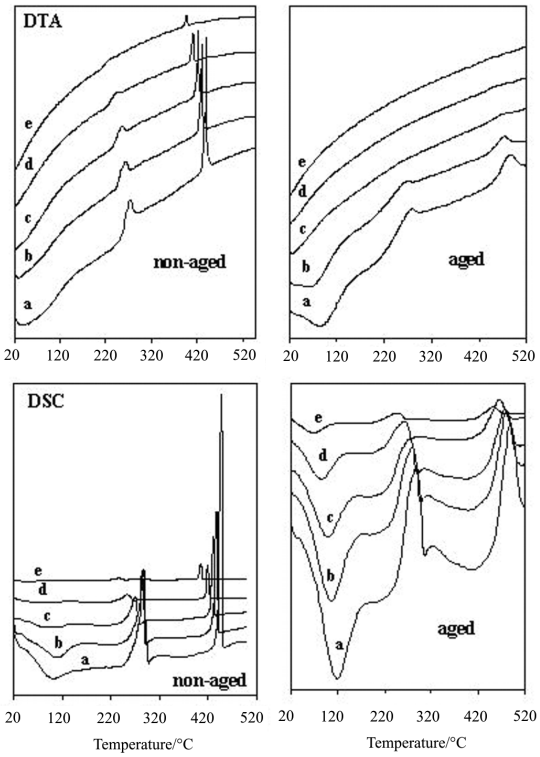

Fig. 4 DTA and DSC curves of the aged and non-aged samples, recorded with various heating rates a – 25°C/min, b – 15°C/min, c – 10°C/min, d – 5°C/min, e – 2°C/min

the temperature range of 400–490°C the glow phenomenon was observed, especially when the heating rate was sufficiently high.

Based on the DTA and DSC curves, recorded with different heating rate for the non- and aged zirconia, a kinetic analysis following the Kissinger's method [35, 36] was performed, assuming first order rate of the invoked processes. In this method the peak maximum temperatures, T_m, and the heating rates, Φ, are related through the following equation: $\ln(\Phi/T^2) = -E_a/RT_{max} + \ln(AR/E_a)$, where A is the pre-exponential factor, R is the gas constant, E_a is the activation energy and $AR/E_a = k$ is the rate constant. Thus, by plotting $\ln(\Phi/T)$ *vs.* $(1/RT_{max})$, the activation energies of the corresponding processes involved in the gel transformation can be evaluated from the slope of the straight lines, associated with each thermal effect (Fig. 5) [37, 38].

The results calculated independently from DTA and DSC profiles are summarized in Table 1. Although these values are formally related to the principal steps of the gel transformation (dehydration, nucleation and coalescence), they only have apparent meaning because mechanistically these steps are quite involved. The E_a values obtained from DSC and DTA curves compare fairly well with each other, with the exception of those corresponding to the coalescence of the aged samples, where the dif-

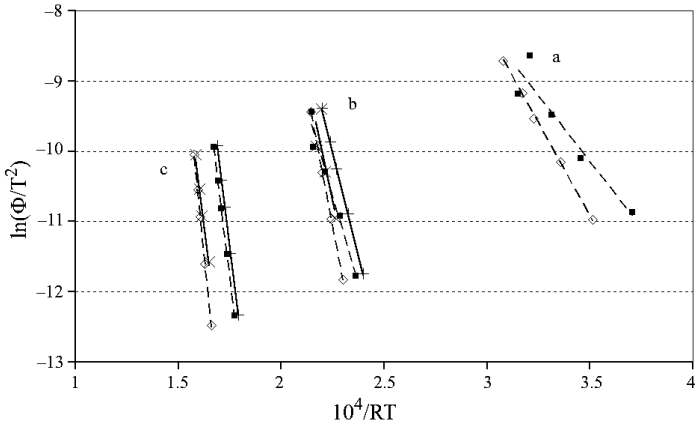

Fig. 5 Kissinger plot for the curves from Fig. 4, a – corresponds to dehydration, b – nucleation and c – to coalescence. (■ – DSC non-aged ZrO_2, ◇ – DSC aged, + – DTA non-aged, × – DTA aged)

Table 1 Activation energies and kinetic constants calculated from DTA and DSC curves for non-aged and aged ZrO_2, obtained from 0.6 M solution of $ZrOCl_2$

Sample and technique	Dehydration E_a/kJ mol^{-1}	Nucleation E_a/kJ mol^{-1}	Coalescence E_a/kJ mol^{-1}
non-aged ZrO_2 DSC	36.6(9)	97.6(7)	233.00(4)
aged ZrO_2 DSC	51.84(8)	150.77(5)	300.7(2)
non-aged ZrO_2 DTA	31.1(9)	117.9(1)	236.3(2)
aged ZrO_2 DTA	40(1)	135(2)	224.4(5)

ferences appeared considerably higher. However in this case the value evaluated from the DSC curves (301 kJ mol^{-1}) is probably more reliable; since it is close to that reported by Maček *et al*. [32]. The values of the activation energies of all transformation steps were higher for the aged ZrO_2 samples than of those obtained for the raw zirconia. This indirectly points to the differences in the molecular and the microstructural properties of both samples confirmed by the corroborative sorption and microscopic measurements. Higher activation energies of the main transformation steps – observed in the case of the aged samples – retard the formation of the oxide and its densification. As a result, these samples exhibit higher surface area and porosity along with better textural properties.

Conclusions

The mechanism of *t*-ZrO_2 formation by precipitation from the aqueous solutions of $ZrOCl_2$ was followed by means of thermal analysis corroborated by XRD and electron

microscopic studies. It was shown that aging of zirconia gel at 100°C for 48 h and the presence of small amounts (~0.05 wt.%) of Si lead to effective metastabilization of tetragonal ZrO_2. Transformation of the zirconia gel into tetragonal zirconium oxide involves three principal mechanistic steps: dehydration, nucleation and coalescence. The nucleation is the most involved process and entails dehydroxylation, oxolation and olation giving rise to complex thermal behavior. From the Kissinger equation apparent activation energies of these processes were determined. It was also shown that aging favors the formation of the well-ordered meso- and micropores structure that leads to a remarkable increase of the specific surface area and pore volume of the resultant oxide.

References

1 T. Yamaguchi, Catal. Today, 20 (1994) 199.
2 P. D. L. Mercera, J. G. van Ommen, E. B. M. Doesburg, A. J. Burggraaf and J. R. H. Ross, Appl. Catal., 71 (1991) 363.
3 K. Sayama and H. Arakawa, J. Phys. Chem., 97 (1993) 532.
4 H. Uchida, M. Yoshida and M. Watanabe, J. Electrochem. Soc., 146 (1999) 1.
5 A. H. Hauer and L. W. Hobbs (Eds), Advances in Ceramics, Vol. 3., Science and Technology of Zirconia, Am. Ceram. Soc., Columbus, OH, 1981.
6 E. M. Logothetis, Automotive Oxygen Sensors, in Chem. Sensors Technol. Vol. 3. (N. Yamazoe Ed.) Kodansha, Tokyo and Elsevier, Amsterdam 1991, p. 83-104.
7 U. Ciesla, D. Demuth, R. Leon, P. M. Petroff, G. D. Stucky, K. Unger and F. Schüth, J. Chem. Soc. Chem. Commun., (1994) 2070.
8 M. J. Hudson and J. A. Knowles, J. Mater. Chem., 6 (1996) 89.
9 J. A. Wang, M. A. Valenzuela, J. Salmones, A. Vázquez, A. García-Ruiz and X. Bokhimi, Catal. Today, 68 (2001) 21.
10 G. K. Chuah, S. H. Liu, S. Jaenicke and J. Li, Microp. Mesop. Mat., 39 (2000) 381.
11 S. Brunauer, P. H. Emmett and E. Teller, J. Am. Chem. Soc., 60 (1938) 309.
12 E. P. Barrett, L. G. Joyner and P. H. Halenda, J. Am. Chem. Soc., 73 (1951) 373.
13 G. Horvath and K. Kawazoe, J. Chem. Soc. Jpn., 16 (1983) 470.
14 E. Tani, M. Yoshimura and S. Sómiya, J. Am. Ceram. Soc., 66 (1983) 11.
15 G. K. Chuah, Catal. Today, 49 (1999) 131.
16 M. Henry, J. P. Jolivet and J. Livage, Struct. Bond., 77 (1992) 155.
17 A. Clearfield, Rev. Pure Appl. Chem., 14 (1964) 91.
18 K. Matsui and M. Ohgai, J. Am. Ceram. Soc., 80 (1997) 1949.
19 Z. Sojka, P. Jakubus, A. Adamski and A. Kotarba, Key Eng. Mater., (in print).
20 T. Mitsuhashi, M. Ichihara and U. Tatsuke, J. Am. Ceram. Soc., 57 (1974) 97.
21 R. C. Garvie, J. Phys. Chem., 69 (1965) 1238.
22 S. J. Gregg and K. S. W. Sing, Adsorption, Surface Area and Porosity, 2nd ed., Academic Press, London 1982.
23 G. Leofanti, M. Padovan, G. Tozzola and B. Venturelli, Catal. Today, 41 (1998) 207.
24 J. Ościk, Adsorption (in Polish), PWN, Warsaw, 1983.
25 F. G. R. Gimblett, A. A. Rahman and K. S. W. Sing, J. Coll. Interf. Sci., 84 (1981) 337.
26 W. Stichert, F. Schüth, Chem. Mater. 10 (1998) 2020.
27 J. Livage, K. Doi and C. Mazières, J. Am. Ceram. Soc., 51 (1968) 349.

28 M. C. Silva, G. Trolliard, R. Guinebretière, A. Dauger and B. Frit, Key Eng. Mat., 132–136 (1997) 264.
29 R. Srinivasan and B. H. Davis, J. Coll. Interface Sci., 156 (1993) 400.
30 A. Christiansen and E. A. Carter, Phys. Rev. B, 58 (1998) 8050.
31 M. A. Blesa, A. J. G. Maroto, S. I. Passagio, N. E. Fizliolia and G. Rigoti, J. Mater. Sci., 20 (1985) 4601.
32 J. Maček, M. Marinšek and B. Novosel, J. Thermal Anal., 48 (1997) 675.
33 A. Kaddouri, J. Therm. Anal. Cal, 53 (1998) 97.
34 R. S. Pavlik, Jr., J. Am. Ceram. Soc., 80 (1997) 1469.
35 H. H. E. Kissinger, Anal. Chem., 29 (1957) 1702.
36 J. Llópiz, M. M. Romero, A. Jerez and Y. Laureiro, Thermochim. Acta, 256 (1995) 205.
37 J. Dweck, R. S. Aderne and D. J. Shanefield, J. Therm. Anal. Cal., 64 (2001) 1163.
38 N. Regnier and S. Fontaine, J. Therm. Anal. Cal., 62 (2001) 789